International Journal of Heat and Mass Transfer 52 (2009) 5081–5089

Contents lists available at ScienceDirect

International Journal of Heat and Mass Transfer

journal homepage: www.elsevier.com/locate/ijhmt

Thermal accommodation coefficients between polyatomic gas molecules and soot in laser-induced incandescence experiments

K.J. Daun *

Department of Mechanical and Mechatronics Engineering, University of Waterloo, 200 University Ave. W. Waterloo, Ont., Canada N2L 3G1

ARTICLE INFO

Article history:
Received 20 November 2008
Received in revised form 16 April 2009
Accepted 16 April 2009
Available online 17 June 2009

Keywords:
LII
Molecular dynamics
Accommodation coefficient
Gas surface scattering
Free molecular conduction

ABSTRACT

Time-resolved laser-induced incandescence demands detailed knowledge of the thermal accommodation coefficient, but to date little is understood about the gas/surface scattering physics underlying this parameter in LII experiments. This paper presents a molecular dynamics (MD) simulation that models polyatomic molecules as rigid rotors and soot as crystalline graphite. A Monte Carlo integration over incident gas molecular speeds and surface atomic vibrational phases yields simulated thermal accommodation coefficients that match the experimentally-measured values. The MD simulation is then extended to assess how α changes with gas and soot temperature, and finally to define a Cercignani–Lampis–Lord scattering kernel that will form a boundary condition in future Monte Carlo simulations of heat and mass transfer between soot aggregates and the surrounding gas.

1. Introduction

Time-resolved laser-induced incandescence (TiRe-LII) is an emerging diagnostic for characterizing both the particle volume fraction and primary particle size in soot-laden aerosols. In this technique a short laser pulse energizes soot particles in the laser path to incandescent temperatures, typically 3000–3600 K in low-fluence experiments, after which the particles cool back to the ambient gas temperature. The time-resolved spectral incandescence of the laser-energized particles is measured at two or more wavelengths throughout the process and the ratio of these signals usually defines a pyrometric temperature. The soot volume fraction is then inferred from the strength of the LII signal [1], and since individual primary particles cool at a rate proportional to their specific surface area, the primary particle size distribution can be found by deconvolving the time-resolved signal decay [2].

The latter calculation relates the pyrometric temperature decay, which indicates the drop in the sensible energy of the particles, to the heat conduction with the surrounding gas. In most TiRe-LII experiments carried out on soot at atmospheric pressures heat conduction occurs in the free-molecular regime, in which the mean free path of the gas is larger than the primary particle diameter. Consequently, the cooling rate depends on the frequency with which gas molecules collide with the hot particle surface and the average energy transfer from the particle surface to the gas molecule at each collision. This latter quantity is specified by the thermal accommodation coefficient,

$$\alpha = \frac{\langle E_o - E_i \rangle}{2k_B(T_s - T_g) + \left[U(T_s) - U(T_g)\right]}, \tag{1}$$

where $\langle E_o - E_i \rangle$ is the average energy transferred from the particle to a gas molecule. The denominator of Eq. (1) is the maximum energy that can be transferred to the translational and internal energy modes of gas molecule, which would occur if the gas molecule equilibrated with a thermal reservoir at T_s.

The thermal accommodation coefficient used to carry out TiRe-LII particle sizing is usually found by performing LII experiments on aerosols containing particles with sizes characterized through thermophoretic sampling and electron microscopy [3–7] or light scattering [8]. Unfortunately, most of these experiments reveal very little about the gas–surface scattering physics that underlies soot particle cooling in the free-molecular regime, largely because a systematic comparison of accommodation coefficients obtained from different studies is precluded by the high degrees of variability and experimental uncertainty in the thermophysical properties and morphology of soot particles. Consequently, most LII researchers treat α more like a fitting constant that is adjusted to obtain "reasonable" particle sizes instead of a parameter having physical meaning in its own right. To date there has been little accord over what constitutes a reasonable value for the thermal accommodation coefficient or how it may change with gas composition and temperature, the latter being particularly important since LII experiments are routinely carried out on aerosols ranging from room temperature to around 2000 K in flames. This uncertainty

* Tel.: +519 888 4567x37871.
E-mail address: kjdaun@mme.uwaterloo.ca

0017-9310/$ - see front matter © 2009 Elsevier Ltd. All rights reserved.
doi:10.1016/j.ijheatmasstransfer.2009.05.006

Nomenclature

A_a	projected aggregate area (m^2)
A_p	projected primary particle area (m^2)
A_{cond}	aggregate heat transfer area (m^2)
c_s	specific heat of soot ($J\,kg^{-1}\,K^{-1}$)
$c_v(T)$	specific heat of gas ($J\,molecule^{-1}\,K^{-1}$)
C_1	Eq. (8) (s^{-1})
d_p	primary particle diameter (m)
E	energy of gas molecule/gas molecular stream ($J\,molecule^{-1}$)
$f(\boldsymbol{v})$	velocity distribution
f_a	fractal pre-factor
$\mathbf{J}$	moment of inertial tensor ($kg\,m^2$)
J	moment of inertia ($kg\,m^2$)
k_B	Boltzmann's constant ($1.38\times10^{-23}\,J\,molecule^{-1}\,K^{-1}$)
m_g	gas molecular mass (kg)
m_s	atomic mass of carbon (kg)
$\boldsymbol{n}$	surface unit normal vector
N''	incident molecular number flux ($molecules\,m^{-2}\,s^{-1}$)
N_p	number of primary particles per aggregate
P_g	gas pressure (kPa)
$R(\boldsymbol{v_o}\|\boldsymbol{v_i})$	scattering kernel
T	temperature (K)
t	time (s)
$\boldsymbol{v}$	gas molecular velocity ($m\,s^{-1}$)
$U(T)$	internal energy (kJ)
$U_{gs}(z)$	gas/surface atomic pairwise potential (kJ)
$W(z)$	potential well (kJ)
α	thermal accommodation coefficient
β	inverse of the most probable speed, $(m_g/2k_BT)^{1/2}$ ($s\,m^{-1}$)
$\delta()$	Kronecker delta
ε_a	fractal exponent
ε_{gs}	Lennard–Jones potential well depth (kJ)
γ^*	adiabatic constant, Eq. (7)
μ	reduced mass (m_g/m_s)
ρ_s	density of soot ($kg\,m^{-3}$)
σ_{gs}	Lennard–Jones potential equilibrium distance (m)
$\boldsymbol{\omega}$	rotational velocity ($rad\,s^{-1}$)
ζ_{rot}	rotational degrees of freedom

Subscripts and superscripts

i, o	incident, scattered
n, t, r	normal, tangential, rotational
s, g	surface, gas
k	Monte Carlo trial number

severely undermines the confidence that can be placed in particle sizes obtained through TiRe-LII.

Daun et al. [7] endeavored to address this shortcoming by measuring α between laser-energized soot particles of known morphology and different gas species. They observed two main trends in the data: first, that α increases with gas molecular mass; and second, that α decreases with increasing structural complexity for gas molecules having similar masses. The former trend was recently duplicated in a classical mechanics-based molecular dynamics simulation of thermal accommodation coefficients for monatomic gases that modeled laser-energized soot as graphite at 3000 K [9].

The latter trend was thought to indicate preferential accommodation of surface energy into the translational energy mode of the gas molecule over the internal (rotational and vibrational) energy modes [7]. This paper presents novel molecular dynamics (MD) results that provide a better physical understanding of the process of thermal accommodation between soot and various polyatomic gases in TiRe-LII experiments. The paper begins with a brief review of the experimental technique used to measure α, followed by a summary of the molecular dynamics model. The MD results are then used to explain how surface energy is accommodated selectively by different energy modes of the gas molecule, and how α varies with gas and surface temperature. Finally, we show how the Cercignani–Lampis–Lord scattering kernel [10,11] can predict the conditional probability of scattered gas molecules having a specified trajectory, speed, and rotation given their incident configuration. In the future this scattering kernel will be applied as a boundary condition in DSMC simulations of heat and momentum transfer between soot particles and the surrounding gas.

2. Experimental method

The experimental apparatus consists of a venturi-driven eductor, an LII measurement system, and an ethylene diffusion flame generated with a co-flow burner operating under conditions described in [1]. Motive gas passes through the venturi and induces a pressure drop that draws soot from the flame, through a sampling manifold, and into the motive gas stream. The soot/gas mixture then enters an LII chamber where the soot particles are heated to peak temperatures between 3000 and 3600 K by a pulsed laser, and the resulting incandescence is imaged onto two photomultipliers equipped with narrow-band interference filters centered at 397 nm and 780 nm, respectively. Transient signals from the photomultipliers are digitized and averaged over 100 shots to mitigate shot noise, resulting in a pair of incandescence decay curves that are used to define a pyrometric temperature decay curve. A more detailed description of the experimental apparatus is provided in [9].

The thermal accommodation coefficient calculation is based on the soot morphology, which is characterized by TEM images of soot sampled from the gas stream entering the LII chamber. The number of primary particles per aggregate is estimated from the 2-D projected area of the aggregate image using the method of Köylü et al. [12]

$$N_p = f_a(A_a/A_p)^{\varepsilon a}, \tag{2}$$

where f_a and ε_a are fractal parameters set equal to 1.16 and 1.1, respectively, typical for soot particles that are mass-fractal in nature [12]. The projected area of the aggregate, A_a, is obtained using image analysis software while that of a single primary particle, $A_p = \pi d_p^2/4$, is derived assuming $d_p = 29$ nm measured from the TEM images of the present study; this value is consistent with a more detailed morphological study of soot sampled from within the flame [13]. Based on a survey of 48 images most soot aggregates contain between 25 and 400 primary particles with an average of around 200 primary particles per aggregate.

The thermal accommodation coefficients are then calculated as follows [5,7]. An energy balance on the soot aggregates shows that the cooling rate after the laser pulse is governed by

$$\rho_s c_s N_p \frac{\pi d_p^3}{6}\frac{dT_s}{dt} = -q_{cond}[T_s(t), T_g], \tag{3}$$

where ρ_s and c_s are the density and specific heat of soot. (Radiation is negligible in experiments carried out in atmospheric pressures, and soot sublimation/evaporation is insignificant in low-fluence LII experiments [14].) The heat conduction is expressed in terms of the thermal accommodation coefficient,

$$q_{cond}[T_s(t), T_g] = \alpha A_{cond} N'' \{2k_B[T_s(t) - T_g] + U(T_s) - U(T_g)\}, \quad (4)$$

where N'' is the incident molecular number flux and A_{cond} is the heat conduction area. The change in internal energy (per molecule) is found from the temperature-dependent specific heat, $c_v(T) = k_B/[\gamma(T) - 1]$,

$$U(T_s) - U(T_g) = k_B\left[\int_{Tg}^{Ts} \frac{dT}{\gamma(T) - 1} - \frac{3}{2}(T_s - T_g)\right], \quad (5)$$

where $\gamma(T)$ is the specific heat ratio. After further substitutions and manipulations [15,16] it can be shown that

$$q_{cond} = \alpha A_{cond} \frac{P_g c(T_g)}{8T_g} \frac{\gamma^* + 1}{\gamma^* - 1}[T_s(t) - T_g], \quad (6)$$

where $c(T_g) = (8k_B T_g/\pi m_g)^{1/2}$ is the mean free speed of the gas molecules, P_g and T_g are taken to be 101.3 kPa and 293 K, and

$$\frac{1}{\gamma^*(T_s, T_g) - 1} = \frac{1}{T_s - T_g}\int_{Ts}^{Tg} \frac{dT}{\gamma(T) - 1}. \quad (7)$$

The thermal accommodation coefficient is derived by substituting Eq. (6) into Eq. (3) and solving to get $\ln\theta(t) = C_1\alpha t + C_2$ with $\theta(t) = T_s(t) - T_g$,

$$C_1 = \frac{3}{4}\frac{A_{cond}}{\rho_s c_s N_p \pi d_p^3}\frac{P_g c(T_g)}{T_g}\frac{\gamma^* + 1}{\gamma^* + 1}, \quad (8)$$

and C_2 as a constant of integration. The accommodation coefficient is then found by performing a linear regression of $\ln\theta(t)$ with respect to t as shown in Fig. 1. At longer cooling times the temperature decay becomes non-exponential due to differential cooling of different-sized particles, while for a brief period immediately after the pulse mechanisms other than free molecular conduction affect the cooling rate [7]. For these reasons, the linear regression is carried out on data sampled between 50 and 100 ns after the laser pulse.

The heat conduction area in Eq. (6) is a major source of uncertainty in the above calculation. Simply setting $A_{cond} = N_p\pi d_p^2$ overestimates the heat transfer area and underestimates α since the aggregate interior is shielded from incident gas molecules by the primary particles on the exterior. In this paper we adopt the treatment of Snelling et al. [5], who estimated $A_{cond} = \pi d_p^2 (N_p/f_a)^{-\varepsilon a}$ based on Eq. (2) following the argument that in the free-molecular regime incident gas molecules follow a straight path over a distance greater than d_p before colliding with the particle surface, so they only "see" the 2-D projected area as they approach the aggregate. Liu et al. [17] found this method to be qualitatively correct based on a detailed DSMC simulation of free molecular heat conduction from soot aggregates, but suggested an improvement that uses quadratic expressions for f_a and ε_a in terms of α to account for gas molecules that partially accommodate and then scatter from exterior primary particles towards the aggregate interior. The previous MD simulation of α between soot and monatomic gases [9] showed that the heat transfer area of Snelling et al. [5] produces better agreement with the simulated values, however, so the experimental data presented in this paper is derived using this value for A_{cond}.

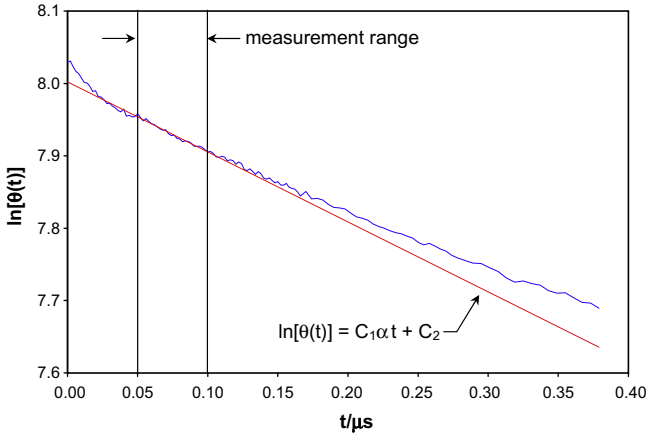

Fig. 1. The thermal accommodation coefficient is calculated from a linear regression of pyrometrically-observed temperature [7].

3. Molecular dynamics simulation

In this work free molecular conduction between the soot particle and gas is simulated by a large number of independent scattering events between gas molecules issuing from an equilibrium gas at 300 K and crystalline graphite at 3000 K, which in turn are modeled using a classical mechanics-based molecular dynamics simulation. Although the experimental results elucidate general trends of α with gas molecular mass and structure [7], the MD simulation provides far more insight into the underlying physics and also allows us to explore regimes that are otherwise difficult to recreate experimentally.

The first step in the simulation is to define interatomic pairwise potentials between the constituent atoms. These potentials are then differentiated with respect to displacement to yield the forces acting on the atoms at any instant, and the resulting set of differential equations are integrated over time using a velocity-verlet algorithm [18] to obtain the atomic trajectories. The graphite model consists of 10 graphene sheets that contain 1500 carbon atoms each. Harmonic boundary conditions are applied around the edges of each sheet, while the bottommost layer is kept rigid to simulate the inertia of the remaining layers. As shown in Fig. 2a, the graphene sheets consist of carbon atoms covalently bonded into a hexagonal lattice, with the sheets connected vertically by comparatively weak Van der Waals forces. The in-plane covalent bonds are represented by harmonic potentials [19], while interplane Van der Waals forces are modeled as Morse potentials between the nearest and next-nearest neighbors shown in Fig. 2b and c [20]. Further details of the graphite model are provided in [9].

Polyatomic gas molecules are modeled as rigid rotors, consisting of point masses separated by fixed bond distances. (A justification for this treatment is discussed later in the paper.) Lennard–Jones 6–12 pairwise potentials are defined between each constituent gas atom and the carbon atoms in the graphite,

$$U_{gs}(r) = 4\varepsilon_{gs}\left[\left(\frac{\sigma_{gs}}{r}\right)^{12} - \left(\frac{\sigma_{gs}}{r}\right)^{6}\right], \quad (9)$$

with potential parameters defined in Table 1 for graphite and nitrogen [21], carbon monoxide [22], nitrous oxide [23], carbon dioxide [24], and methane and ethane [25].

Each gas/surface scattering simulation starts by initializing the carbon atoms with random displacements and velocities. The graphite is then warmed up using an Andersen thermostat [26] to maintain a mean surface temperature of 3000 K. The atomic trajectories are calculated using a finite time step is 0.35 fs, or about 1% of the characteristic oscillation period of the graphite lattice. The thermostat is deactivated after 40 time steps and the gas molecule is then introduced into the simulation $10\sigma_{gs}$ above the uppermost graphene sheet, where the potential well is negligible. Translational and rotational velocities of the gas molecule are sampled from a Maxwell-Boltzmann distribution at 300 K, while the orientation is set according to randomly-chosen Euler angles. The molecule accelerates towards the surface due to the potential well, collides with the surface, and then scatters back to the surrounding gas; in some cases it scatters immediately, while other times it "chatters" over the surface until it receives enough normal translational energy to overcome the potential well. The simulation

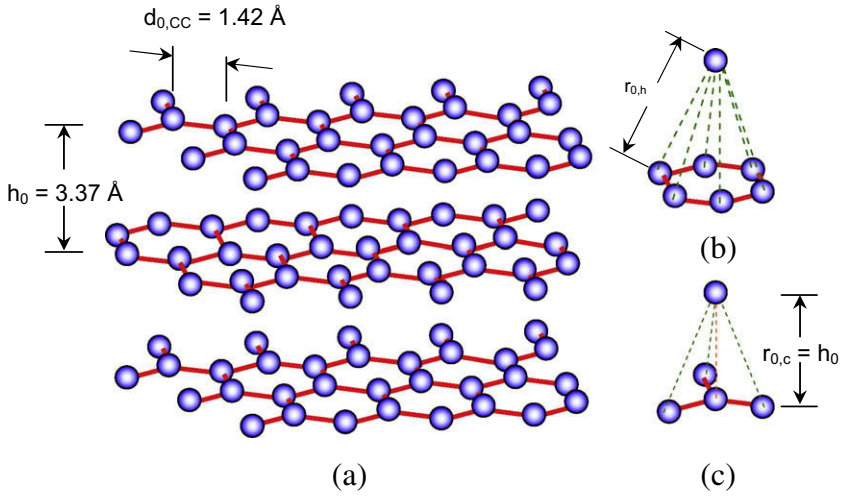

Fig. 2. Graphite consists of layers of covalently-bonded carbon atoms in a hexagonal lattice. Each covalent bond (a) is modeled by a harmonic potential and (b and c) the interplane Van der Waals forces are simulated using pairwise Morse potentials between nearest neighbors [9].

terminates once the retreating gas molecular velocity becomes constant.

Solving the equations of motion for rigid polyatomic gas molecules is complicated by the fact that the linear molecules considered in this study (N_2, CO, N_2O, and CO_2) have a null moment of inertia about the molecular axis resulting in a singular moment-of-inertia tensor that cannot be inverted directly. We avoid this problem by decomposing the motion of the rigid gas molecule into translational and rotational components in a molecular reference frame aligned with the principle moments-of-inertia following Evans [27], and then solve the coupled Euler equations using velocity-verlet integration.

Each simulated gas–surface scattering event is an independent trial of a Monte Carlo integration over incident molecular trajectories and surface atomic phases. After a large number of simulations the energy transferred from the vibrating surface atoms to the gas molecules is defined by α, which is evaluated according to Eq. (1). The MD simulation also provides insight into the efficiency of energy transfer into different energy modes of the gas molecule through corresponding accommodation coefficient components. Surface energy transfer into the normal- and tangential-translational modes of the gas molecule is quantified by normal-translational and tangential-translational accommodation coefficients [10,11],

$$\alpha_n = \frac{\langle E_{o,n} - E_{i,n}\rangle}{k_B(T_s - T_g)} = \frac{1/2 m_g \langle v_{o,n}^2 - v_{i,n}^2\rangle}{k_B(T_s - T_g)} \tag{10}$$

Table 1
Lennard-Jones parameters for pairwise potentials between atoms of the gas molecule and carbon atoms in the graphite.

Species	Atomic pair	ε_{gs} (K)	σ_{gs} (Å)	Ref.
N_2	N–gr	32.4	3.36	[21]
CO	C–gr	34.8	3.39	[22]
	O–gr	41.2	3.14	
N_2O	N–gr	34.5	3.36	[23][a]
	O–gr	41.2	3.14	
CO_2	C–gr	47.5	3.22	[24][b]
	O–gr	28.1	3.08	
CH_4, C_2H_6	C–gr	27.1	3.47	[25][c]
	H–gr	26.8	2.99	

[a] Pairwise LJ parameters for N_2 and CO [22] were adapted to N_2O.
[b] Calculated by applying Lorentz–Berthelot combining rules to carbon-graphite and oxygen-graphite adsorption potentials.
[c] LJ parameters are best-fit to correlations derived from extended Hückel theory.

and

$$\alpha_t = \frac{\langle E_{o,t} - E_{i,t}\rangle}{k_B(T_s - T_g)} = \frac{1/2 m_g \langle v_{o,t}^2 - v_{i,t}^2\rangle}{k_B(T_s - T_g)} \tag{11}$$

respectively [10,11], while energy transfer into the rotational modes is described by the rotational accommodation coefficient,

$$\alpha_r = \frac{\langle E_{o,r} - E_{i,r}\rangle}{\zeta_r/2 k_B(T_s - T_g)} = \frac{1/2\langle \boldsymbol{\omega}_o^T \mathbf{J}_o \boldsymbol{\omega}_o - \boldsymbol{\omega}_i^T \mathbf{J}_i \boldsymbol{\omega}_i\rangle}{\zeta_r/2 k_B(T_s - T_g)}, \tag{12}$$

[11] where $\mathbf{J}$ is the moment-of-inertia tensor of the gas molecule, ω is the rotational velocity vector, and ζ_r is the number of rotational degrees of freedom. For linear molecules (N_2, CO, N_2O, and CO_2) $\zeta_r = 2$, while for nonlinear molecules (CH_4 and C_2H_6) $\zeta_r = 3$.

A major uncertainty in the above procedure is the representation of soot using crystalline graphite. While the structure of soot is certainly is not identical to graphite, it has been speculated that graphene crystallates, the main constituent of soot primary particles, anneal at around 2500 K to form multishell fullerines that resemble the laminate structure of crystalline graphite [28], which may make graphite a reasonable surrogate for soot in LII experiments. The graphite half-plane likely overestimates the true potential between an incident gas molecule and soot primary particles; this may have a pronounced effect on the trajectory of heavier, slowly-moving molecules like Krypton and Xenon [9], but does not play an important role for the lighter species considered in the present study. The finite dimension of the primary particles also suppresses formation of long wavelength surface phonons [9], but again these are more pronounced for slower, heavier gas molecules and not the species considered in this study.

4. Results and discussion

4.1. Comparison of MD and experimental results

The MD simulation is first validated by comparing simulated accommodation coefficients to the experimentally-measured values in [7] and the simulated α values for monatomic gasses [9] as a function of reduced mass, $\mu = m_g/m_s$. These results are plotted in Fig. 3; error bars are omitted for clarity, but the average MD results have standard errors less than 5% while the experimental uncertainty is as much as 50% due to uncertainties in the properties used to calculate α [7].

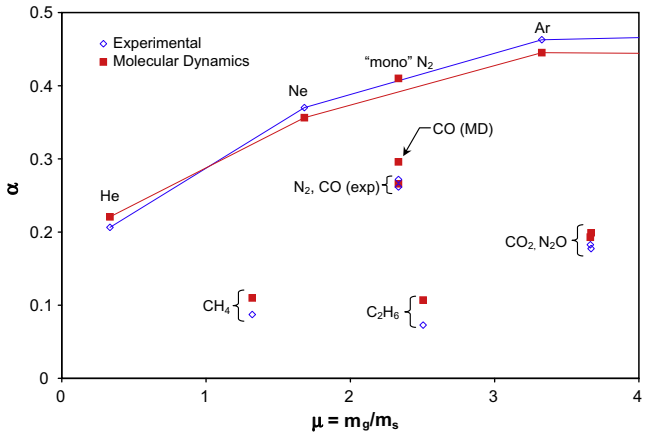

Fig. 3. Simulated accommodation coefficients for polyatomic gases, plotted with simulated values for monatomic gases [9] and experimental data [7].

Fig. 3 shows good agreement between the simulated and experimentally-measured accommodation coefficients; moreover, the difference in magnitude between accommodation coefficients for monatomic and polyatomic gases observed in the experimental study [7] is reproduced by the MD simulation. The fact that this level of agreement is obtained by treating polyatomic molecules as rigid rotors is strong evidence that surface energy accommodation into the vibrational energy modes of the gas molecules is negligible. Polyatomic molecules have lower accommodation coefficients compared to monatomic molecules having similar mass because the denominator of Eq. (1) corresponds to the case where all energy modes equilibrate with the surface temperature, while only the translational and rotational modes seem to be accessible to the vibrating surface atoms. Moreover, if significant surface energy were accommodated into the vibrational modes of the gas molecules, one would expect it to occur in different amounts for N_2O and CO_2 given their differing vibrational levels, but Fig. 3 shows that the accommodation coefficients for these two species are very similar. To further demonstrate how the internal energy modes of the gas molecule affect overall thermal accommodation, a hypothetical monatomic N_2 molecule was conceived having the same mass and desorption energy of diatomic nitrogen but with no internal degrees of freedom. As shown in Fig. 3, the thermal accommodation coefficient for this molecule lies along the trend line for the noble gas thermal accommodation coefficients, further evidence that the lower α values for polyatomic gases is due to ineffective accommodation of surface energy into the internal energy modes of the gas molecule.

In gas/surface scattering the vibrational energy modes of gas molecules are most often accessed through one of two mechanisms [29–31]: gas molecules having a large incident velocity (which is often the case in molecular beam experiments) can have some of their translational kinetic energy redistributed to internal modes through the collision; and alternatively, gas molecules with lower incident energy can follow a trapping/desorption channel, which allows time for the gas molecules to equilibrate with the surface. Neither scenario applies in this system, however, since incident gas molecules effusing from a gas at 300 K have low incident translational energy (and very few of them are vibrationally excited), while the high surface temperature relative to the potential well prevents the gas molecules from becoming adsorbed onto the surface. Fig. 4 shows that the majority of molecules considered in this study undergo at most one or two hops before leaving the surface, which is insufficient for surface energy to enter the vibrational energy mode of the gas molecule.

Further insight is found by plotting the thermal accommodation coefficient components for the gas species considered in this study. The relative magnitudes of α_n, α_t, and α_r in Figs. 5–7, respectively, indicate that most of the accommodated surface energy enters the normal-translational mode of the gas molecule followed by the rotational mode and then the tangential-translational mode, which is consistent with relative accommodation levels observed in molecular beam scattering experiments involving diatomic gas/graphite systems [31]. Fig. 5 shows that α_n follows the same increasing trend with μ for both the monatomic and polyatomic gas molecules, which suggests that molecular structure has little influence on this parameter. Instead, the energy transfer efficiency is governed by surface phonon excitation in the uppermost graphene sheet by the colliding gas molecules. The heavier, slower-moving molecules excite fewer surface phonons and consequently retain more of their incident normal kinetic energy after the collision compared to the lighter, faster molecules.

A comparison of Figs. 5 and 6 shows that α_t is smaller than α_n for all gas species except helium. (The large α_t value for helium is likely due to its relatively small inertia, which makes it easier to accelerate tangentially due to a "glancing blow" from a surface atom.) In contrast to α_n, molecular structure affects α_t since the molecules having more elongated structures (CO_2, N_2O, and C_2H_6) also have larger tangential translational accommodation coefficients compared to those that are more structurally-isotropic.

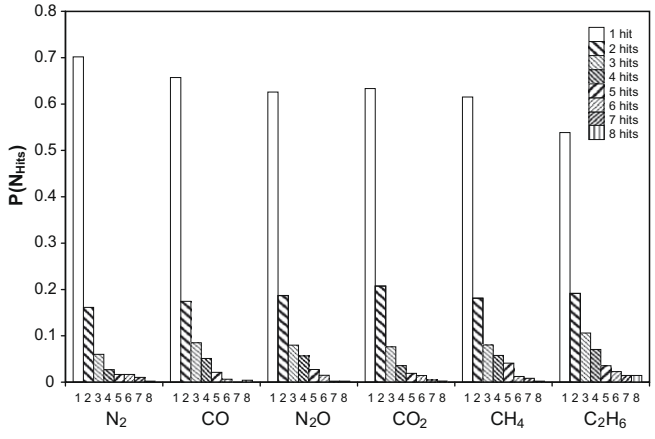

Fig. 4. Probability of an incident gas molecule scattering after N_{hits} with the surface (N_{hits} = 1 is direct scattering).

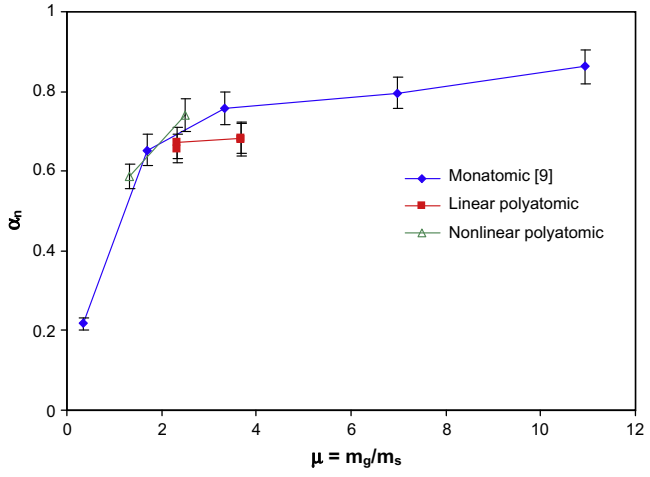

Fig. 5. Plot of α_n for different gas species. (Error bars denote one standard deviation of the mean.)

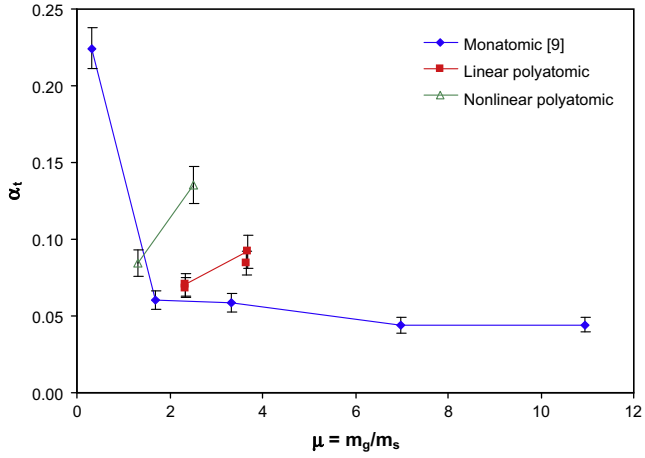

Fig. 6. Plot of α_t for different gas species. (Error bars denote one standard deviation of the mean.)

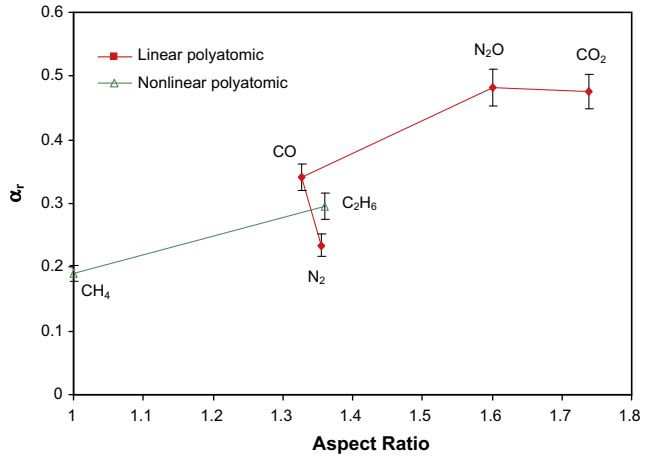

Fig. 7. Plot of α_r for different gas species. (Error bars denote one standard deviation of the mean.)

Structural anisotropy has an even more pronounced effect on the rotational accommodation coefficient, α_r, which has also been observed in other studies (e.g. [32–36]). We demonstrate this trend by plotting α_r versus the aspect ratio of the gas molecule's Van der Waals surface, which is analogue to the ellipticity parameter in hard-ellipsoid models of gas–surface interactions [33,34]. Fig. 7 confirms that α_r increases with the structural anisotropy of the gas molecule.

As noted above, some molecular beam experiments involving other gas/surface scattering systems show that the collision with the surface enables a redistribution of energy between the active degrees of freedom of the gas molecule, particularly between the normal-translational and rotational modes (e.g. [35–38]). We investigate this phenomenon by calculating Spearman's rank-correlation coefficients for 480 independent Monte Carlo trials of the incident and scattered normal-translational, tangential-translational, and rotational energies for carbon dioxide. (Values of ±1 indicate strong correlation while those near zero indicate weak or negligible correlation.) Table 2 shows little evidence of strong translational-rotational coupling in this system, which may be due to the heightened role the oscillating surface atoms play in determining the outgoing trajectory of the gas molecule compared to the molecular beam experiments, which are carried out at lower surface temperatures. There is, however, a strong correlation between $E_{t,i}$ and $E_{t,o}$, which one would expect given the small degree of tangential accommodation seen in Fig. 6.

Table 2
Spearman's rank correlation coefficient between incident and scattered energy components of CO_2, T_g = 300 K.

	$E_{o,n}$	$E_{o,t}$	$E_{o,r}$
$E_{i,n}$	0.081	−0.145	0.019
$E_{i,t}$	−0.049	0.563	0.023
$E_{i,r}$	0.101	0.0204	0.095

4.2. Effect of gas temperature on thermal accommodation

As noted above, the behavior of α with respect to T_g is of great interest to the LII community, since most time-resolved LII experiments are either carried out on soot within flames where T_g is between 1500 K and 2000 K, or on soot-laden aerosols near room temperature. While it is difficult to conceive of a single experimental apparatus that could produce soot-laden aerosols with temperatures spanning this range, the MD simulation can be used to see how α and its components vary with gas temperature. Fig. 8 shows that while α_n increases slightly and α_r drops slightly between 300 K and 1500 K, both α_t and the overall accommodation coefficient, α, remain nearly constant over this range. From 1500 K to 2500 K α_n, α_r, and α all drop with increasing T_g, while α_t increases from 2000 K to 2500 K, although the increase is comparable in size to the variance in the results. Nevertheless, the variation of α over the entire temperature range is small compared to other experimental uncertainties in TiRe-LII.

More physical insight is gained by plotting the average scattered energy components of the gas molecule as a function of the corresponding incident energy components. Fig. 9 shows that while $\langle E_{n,o}\rangle$ increases monotonically with increasing $\langle E_{n,i}\rangle$, the difference between $\langle E_{n,o}\rangle$ and $\langle E_{n,i}\rangle$ drops. (The rate of this drop relative to the change in $T_s - T_g$ determines whether α_n increases or decreases with increasing T_g.) This is consistent with the hypothesis that the gas molecule retains less of its incident normal translational energy due to increasing surface phonon generation with increasing normal incident velocity, as described above. In contrast, tangential-translational kinetic energy is nearly conserved, since $\langle E_{i,t}\rangle \approx \langle E_{o,t}\rangle$ at all gas temperatures and hence α_t values are usually quite low.

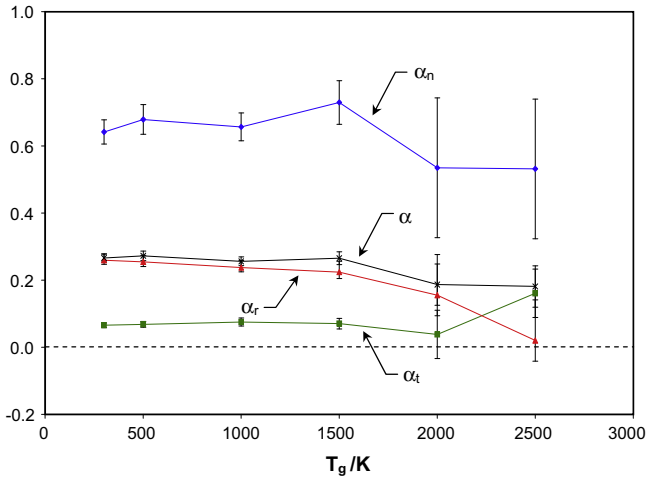

Fig. 8. Simulated thermal accommodation coefficients for nitrogen as a function of temperature. (Error bars denote one standard deviation of the mean.)

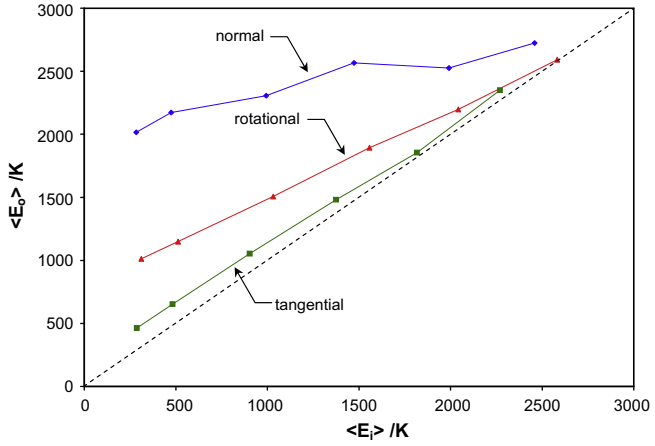

Fig. 9. Average scattered energy of nitrogen as a function of average incident energy at different gas temperatures.

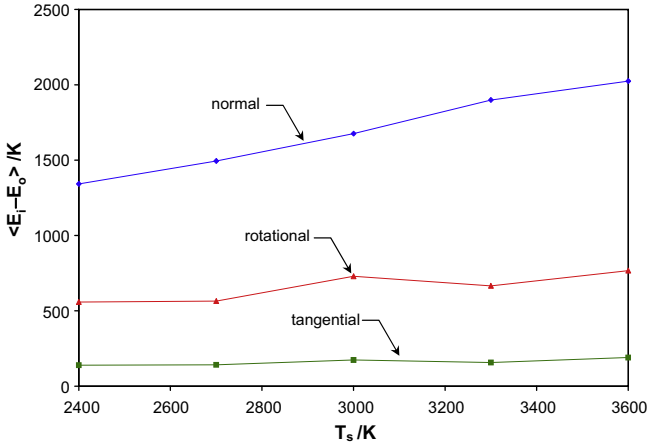

Fig. 10. Average scattered energy of nitrogen as a function of surface temperature.

Fig. 9 also shows that $\langle E_{r,o} \rangle$ varies linearly with the corresponding incident value. This trend has also been observed in other studies, notably Häger et al. [36] who measured the scattering of NO molecular beams having energies ranging from 20 K and 650 K incident on graphite surfaces between 150 K and 600 K. They found that NO molecules either absorb and then reemit diffusely or scatter immediately in a specular manner. Of those that scatter specularly, the average rotational energy depends on the incident rotational energy with a constant slope of roughly 0.5 and an intercept that increases with T_s. For any given surface temperature, then, there exists a critical gas temperature below which the incident gas molecules, on average, undergo rotational heating and above which they undergo rotational cooling. In this study we observe the same linear trend, but with a slope of 0.67. (The difference in slope may be due to the fact that Hägar et al. [36] considered a molecular beam of 45° incidence, while in this work incident gas molecules effuse from an equilibrium gas.) Fig. 9 shows that the critical temperature lies around 2500 K, so for gas temperatures encountered in most LII experiments nitrogen molecules will always undergo slight rotational heating.

4.3. Effect of surface temperature

The effect of changing soot temperature on α is also an important question for TiRe-LII particle sizing, since in low-fluence experiments incandescence is measured as the soot particles cool typically from around 3600 K to 2400 K. Unfortunately, it is again hard to conceive of an LII-based experiment that could provide this information, so Michelsen [31] extrapolated published data from molecular beam experiments involving graphite to conditions typical of LII experiments in an attempt to infer how α may change with T_s. These extrapolations predicted low levels of vibrational accommodation, and that the accommodation of surface energy into the rotational and translational energy modes of gas molecules should "saturate" at high surface temperatures. Since the denominator of Eq. (1) increases linearly with T_s for a fixed T_g, Michelsen [31] proposed an algebraic model for $\alpha(T_s)$ that has the accommodation coefficient increasing as laser-energized soot particles cool to the surrounding gas temperature.

The MD results for nitrogen molecules effusing from an equilibrium gas at 300 K in Fig. 10 show that the energy contained in the three modes increases in a linear way with respect to T_s over temperature ranges typical of low-fluence LII, albeit with small slopes that may be indicative of the saturation behavior observed in molecular beam experiments. Nevertheless, Fig. 11 shows that these slopes are large enough that the accommodation coefficients obtained in this study may be modeled as constant throughout the measured particle cooling period, as is the current standard practice.

4.4. Application of the CLL kernel

Finally, the MD results are used to define a scattering kernel that specifies the conditional probability that a gas molecule having an incident translational and rotational velocity will scatter with a given outgoing translational and rotational velocity. These kernels form the boundary conditions for DSMC simulations of momentum and heat transfer between soot aggregates and the surrounding gas. All such simulations to date either assume that gas molecules thermally equilibrate with the surface [39], or that they are absorbed and reemitted from the surface diffusely with a probability of α and scatter in a specular-adiabatic matter with a probability of $1-\alpha$ [40,16,17]. The latter scenario corresponds to the Maxwell kernel

$$R(\boldsymbol{v}_o|\boldsymbol{v}_i) = (1-\alpha)\delta[\boldsymbol{v}_i - \boldsymbol{v}_o + 2\boldsymbol{n}(\boldsymbol{n}\cdot\boldsymbol{v}_o)] + f_s(\boldsymbol{v}_o)|\boldsymbol{n}\cdot\boldsymbol{v}_o|, \qquad (13)$$

where $\boldsymbol{n}$ is the unit outward normal vector from the surface and f_s denotes the M–B distribution at T_s. Since the Maxwell kernel does not explicitly include a treatment for internal accommodation the

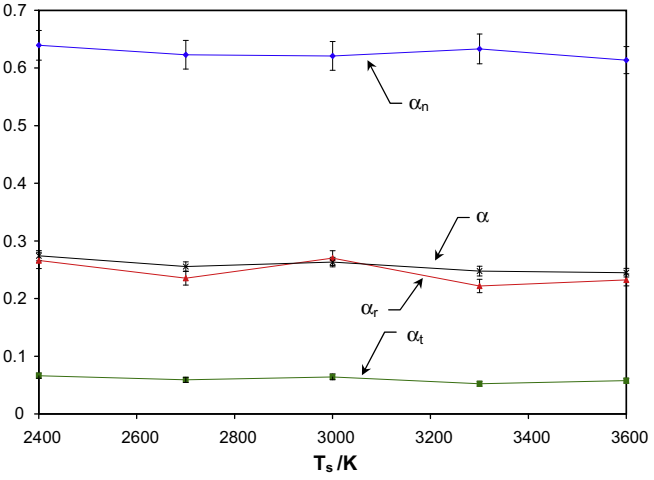

Fig. 11. Simulated thermal accommodation coefficients for nitrogen as a function of surface temperature. (Error bars denote one standard deviation of the mean.)

majority of DSMC simulations involving soot assume a monatomic gas, although Liu et al. [17] used an analogy of Eq. (13) in their study where the internal energy remained unchanged with a probability of $1-\alpha$ and was sampled from a M–B distribution corresponding to T_s with a probability of α.

In our MD simulations of graphite/monatomic gas systems [9] we showed the Cercignani–Lampis–Lord (CLL) kernel [10,11] to be a more realistic treatment of the speeds and trajectories of scattered molecules than the Maxwell kernel. The CLL kernel is given by

$$R(v_o^*|v_i^*) = \frac{2v_{o,n}^{*2}}{\alpha_n\alpha_t} I_0\left(\frac{2\sqrt{1-\alpha_n}}{\alpha_n} v_{o,n}^* \cdot v_{i,n}^{**}\right) \times \exp\left[-\frac{v_{o,n}^{*2}+(1-\alpha_n)v_{i,n}^{*2}}{\alpha_n} - \frac{(\boldsymbol{v}_{o,t}^* + \sqrt{1-\alpha_t}\boldsymbol{v}_{i,t}^*)^2}{\alpha_t}\right], \tag{14}$$

where $\boldsymbol{v}_i^*$ and $\boldsymbol{v}_o^*$ denote the incident and scattered molecular velocities normalized by the most probable speed at the surface temperature, $(2k_BT_s/m_g)^{1/2}$. The CLL kernel assumes that normal- and tangential- translational accommodation are independent processes, which we demonstrate to be the case in Table 2. (Eq. (14) often appears in a slightly different form because Cercignani and Lampis [10] originally used α_t to represent the tangential accommodation coefficient for momentum, not energy. Lord [11] showed that the kernel can be rewritten so that α_n and α_t are both true thermal accommodation coefficients.) A drawback to this kernel is there is often little information about what values α_n and α_t should hold, other than the fact that $\alpha = (\alpha_n + \alpha_t)/2$ for monatomic gases; consequently, in many studies these accommodation coefficients are treated as fitting parameters, and not constants that have physical meaning in their own right. In our previous work [9] we showed how α_n and α_t can be found from Eqs. (10) and (11), resulting in a CLL kernel that accurately reproduced the distribution of scattered molecules for an incident monochromatic molecular beam as well as molecules incident from an equilibrium gas.

In this study we extend this treatment to predict the distribution of rotational energies of scattered linear molecules. Lord [11,41] shows that the conditional probability of linear polyatomic molecules scattering with a given rotational speed is

$$f(\omega_o^{*2}|\omega_i^{*2}) = \frac{1}{\alpha_r}\exp\left[-\frac{\omega_o^{*2}+(1-\alpha_r)\omega_i^{*2}}{\alpha_r}\right]\cdot I_0\left[-\frac{2\sqrt{(1-\alpha_r)\omega_i^{*2}\omega_o^{*2}}}{\alpha_r}\right], \tag{15}$$

where ω_i^* and ω_o^* are the incident and scattered rotational speed normalized by the most probable rotational speed at the surface temperature, $(2k_BT_s/J)^{1/2}$. (The treatment for nonlinear molecules is more complicated and not discussed here.) If the incident molecules effuse from an equilibrium gas at T_g, the CLL kernel predicts that the distribution of scattered molecular speeds conform to a two-temperature Maxwell distribution [42],

$$f(x\beta_x) = x\beta_x \exp(-x^2\beta_x^2), \tag{16}$$

where $x = v_{o,n}$, $\boldsymbol{v}_{o,t}$, or ω_o, and β_x is the inverse of the corresponding most probable translational or rotational speed evaluated at $T_x = \alpha_xT_s + (1-\alpha_x)T_g$. For example, $\beta_n = (m_g/2k_BT_n)^{1/2}$ with $T_n = \alpha_nT_s + (1-\alpha_n)T_g$. Continuous distributions of scattered normal, tangential, and rotational velocities normalized by β_x are obtained by fitting cubic splines to the cumulative density functions of the MD results and then taking the derivative following the procedure described in [9]. Fig. 12 shows that the distributions of the scattered normal, tangential, and rotational velocity all agree with Eq. (16).

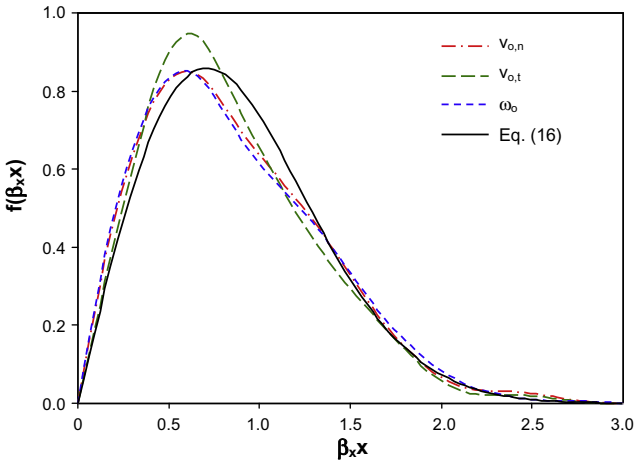

Fig. 12. Distributions of scattered normal, tangential, and rotational speeds of nitrogen normalized by the corresponding most probable speeds. (T_g = 300 K.)

5. Conclusions

Particle sizing through time-resolved laser-induced incandescence relies on the thermal accommodation coefficient, which specifies how efficiently energy is transferred when an incident gas molecule collides with the particle surface. The physics of this parameter in LII experiments is largely unknown, however, and there is little consensus over what constitutes a reasonable value or how this value is influenced by changing experimental conditions. This uncertainty must be rectified before time-resolved LII can mature into a reliable particle sizing technique.

While some information about α has been found through experiment, a molecular dynamics simulation provides far more in-depth understanding of the gas/surface scattering underlying free molecular heat conduction. This study models gas molecules as rigid rotors and neglects their vibrational energy modes. The simulated and experimentally-measured accommodation coefficients are in good agreement, which shows that the lower values of α observed for polyatomic gases is primarily due to negligible energy accommodation into the vibrational mode of the gas molecule. The simulations also show that surface energy is preferentially accommodated into the normal-translational mode of the gas molecule followed by the rotational energy modes; with the exception of helium, very little energy is accommodated into the tangential-translational mode.

The MD simulation is then used to predict how gas and surface temperatures affect the thermal accommodation coefficient. The results for nitrogen show that α remains nearly constant as T_g increases from 300 K to 1500 K and then drops with further increase in T_g, primarily due to a drop in α_n and α_r. Plotting the average energy components of the scattered molecules against the incident molecules as a function of gas temperature shows that both $\langle E_{r,o}\rangle$ and $\langle E_{t,o}\rangle$ increase linearly with their respective incident components, while the difference between $\langle E_{n,o}\rangle$ and $\langle E_{n,i}\rangle$ grows smaller as the incident molecular speed increases. This trend is caused by a greater amount of normal-translational energy of the incident molecule being converted into surface phonons with increasing incident molecular speed. The energy transferred to the scattered molecules is a much weaker function of T_s compared to T_g, and the MD simulation suggests that α may be modeled as constant as laser-energized particles cool back to the gas temperature.

Finally, the accommodation coefficient components obtained from the MD simulation are used to define a Cercignani–Lampis–Lord scattering kernel. For incident molecules effusing from an equilibrium gas the CLL kernel predicts that the outgoing molecules will obey a two-temperature Maxwell distribution, which is

observed to be the case for the MD-simulated gas molecular trajectories.

In the near future, the CLL kernel will be used as a boundary condition in a DSMC simulation to assess the influence of aggregate structure on overall heat and momentum transfer rates from soot particles immersed in polyatomic gases.

Acknowledgements

The author is grateful for the mentorship and helpful discussions with Drs. Greg Smallwood and Fengshan Liu at the National Research Council Canada. This work was made possible by the facilities of the Shared Hierarchical Academic Research Computing Network (SHARCNET:http://www.sharcnet.ca).

References

[1] D.R. Snelling, G.J. Smallwood, F. Liu, Ö.L. Gülder, W.L. Bachelo, A calibration-independent laser-induced incandescence technique for soot measurement by detecting absolute light intensity, Appl. Optics 44 (2005) 6773–6785.
[2] F. Liu, B.J. Stagg, D.R. Snelling, G.J. Smallwood, Effects of primary soot particle size distribution on the temperature of soot particles heated by a nanosecond pulsed laser in an atmospheric laminar diffusing flame, Int. J. Heat Mass Transfer 49 (2006) 777–788.
[3] S.-A. Kuhlmann, J. Reimann, S. Will, On heat conduction between laser-heated nanoparticles and a surrounding gas, J. Aerosol Sci. 37 (2006) 1696–1716.
[4] R. Starke, B. Kock, P. Roth, Nano-particle sizing by laser-induced incandescence (LII) in a shock wave reactor, Shock Waves 12 (2003) 351–360.
[5] D.R. Snelling, F. Liu, G.J. Smallwood, Ö.L. Gülder, Determination of the soot absorption function and thermal accommodation coefficient using low-fluence LII in a laminar coflow ethylene diffusion flame, Combust. Flame 136 (2004) 180–190.
[6] A.V. Eremin, E.V. Gurentsov, M. Hofmann, B.F. Kock, C. Schulz, TR-LII for sizing of carbon particles forming at room temperature, Appl. Phys. B 83 (2006).
[7] K.J. Daun, G.J. Smallwood, F. Liu, Investigation of thermal accommodation coefficients in time-resolved laser-induced incandescence, J. Heat Transfer 130 (12) (2008) 1–9.
[8] T. Lehre, B. Jungfleisch, R. Suntz, H. Bockhorn, Size distributions of nanoscaled particles and gas temperatures from time-resolved laser-induced incandescence measurements, Appl. Optics 42 (2003) 2021–2030.
[9] K.J. Daun, G.J. Smallwood, F. Liu, Molecular dynamics simulations of translational thermal accommodation coefficients for time-resolved LII, Appl. Phys. B 94 (2009) 30–49.
[10] C. Cercignani, M. Lampis, Kinetic models for gas–surface interactions, Trans. Theory Stat. Phys. 1 (1971) 101–114.
[11] R.G. Lord, Some extensions to the Cercignani–Lampis gas–surface scattering kernel, Phys. Fluids A 3 (1991) 706–710.
[12] Ü.Ö. Köylü, C.S. McENally, D.E. Rosner, L.D. Pfefferle, Simultaneous measurements of soot volume fraction and particle size/microstructure in flames using a thermophoretic sampling technique, Combust. Flame 110 (1997) 494–507.
[13] K. Tian, F. Liu, K.A. Thomson, D.R. Snelling, G.J. Smallwood, D. Wang, Distribution of the number of primary particles of soot aggregates in a nonpremixed laminar flame, Combust. Flame 138 (2004) 195–198.
[14] G.D. Yoder, P.K. Diwakar, D.W. Hahn, Assessment of soot particle vaporization effects during laser-induced incandescence with time-resolved light scattering, Appl. Optics 44 (2005) 4211–4219.
[15] A.V. Filippov, D.E. Rosner, Energy transfer between an aerosol particle and gas at high temperature ratios in the Knudsen transition regime, Int. J. Heat Mass Transfer 43 (2000) 127–138.
[16] F. Liu, K.J. Daun, D.R. Snelling, G.J. Smallwood, Heat conduction from a spherical nano-particle: status of modeling heat conduction in laser-induced incandescence, Appl. Phys. B 83 (2006) 355–382.
[17] F. Liu, M. Yang, F.A. Hill, D.R. Snelling, G.J. Smallwood, Influence of polydisperse distributions of both primary particle and aggregate size on soot temperature in low-fluence LII, Appl. Phys. B 83 (2006) 383–395.
[18] D. Frenkel, B. Smit, Understanding Molecular Simulation: From Algorithms to Applications, second ed., Academic Press, San Diego, CA, 2002. p. 75.
[19] L.K. Cohen, A lower bound on the loss of graphite by atomic oxygen attack at asymptotic energy, J. Chem. Phys. 99 (1993) 9652–9663.
[20] M.B. Någård, P.U. Andersson, N. Marković, J.B.C. Pettersson, Scattering and trapping dynamics of gas–surface interactions: theory and experiments for the Xe–graphite system, J. Chem. Phys. 109 (1998) 10339–10349.
[21] M.J. Bojan, W.A. Steele, Interactions of diatomic molecules with graphite, Langmuir 3 (1987) 1123–1127.
[22] C. Peters, M. Klein, Monte Carlo calculations for solid CO and N2 overlayers physisorbed on graphite, Mol. Phys. 54 (4) (1985) 895–909.
[23] B. Leinböck, B. Krömker, H. Wiechert, M. Hoffman, Orientational ordering of N2O molecules adsorbed on graphite (0 0 0 1): a novel commensurate pinwheel structure, Phys. Rev. Lett. 84 (2000) 1954–1957.
[24] X. Zhao, J.K. Johnson, An effective potential for adsorption of polar molecules on graphite, Mol. Simulat. 31 (2005) 1–10.
[25] C. Vidal-Madjar, C. Minot, Adsorption potential of alkanes on graphite, J. Phys. Chem. 91 (1987) 4004–4011.
[26] H.C. Andersen, Molecular dynamics at constant pressure and/or temperature, J. Chem. Phys. 72 (1980) 2384–2393.
[27] D.J. Evans, On the representation of orientation space, Mol. Phys. 34 (1977) 317–325.
[28] H.A. Michelsen, Understanding and predicting the temporal response of laser-induced incandescence from carbonaceous particles, J. Chem. Phys. 118 (15) (2003) 7012–7045.
[29] M.B. Någård, M. Marković, J.B.C. Pettersson, Scattering and trapping dynamics of gas–surface interactions: vibrational excitation of CF3Br on graphite, J. Chem. Phys. 109 (23) (1998) 10350–10360.
[30] C.T. Rettner, F. Fabre, J. Kimman, D.J. Auerbach, Observations of direct vibrational excitation in gas–surface collisions: NO on Ag(1 1 1), Phys. Rev. Lett. 55 (18) (1985) 1904–1907.
[31] H.A. Michelsen, Derivation of a temperature-dependent accommodation coefficient for use in modeling laser-induced incandescence of soot, Appl. Phys. B 94 (2009) 103–117.
[32] W.L. Nichols, J.H. Weare, Heteronuclear diatomic scattering from solid surfaces: a hard cube model, J. Chem. Phys. 63 (1) (1975) 379–383.
[33] T. Kondo, D. Mori, R. Okada, M. Sasaki, S. Yamamoto, A molecular-beam study of the collision dynamics of methane and ethane upon a graphitic monolayer on Pt(1 1 1), J. Chem. Phys. 123 (11) (2005) 114712.
[34] T. Kondo, H.S. Kato, T. Yamada, S. Yamamoto, M. Kawai, Rainbow scattering of CO and N2 from LiF(0 0 1), J. Chem. Phys. 122 (24) (2005) 244713.
[35] J.A. Stinnett, R.J. Madix, Molecular adsorption of alkanes on platinum surfaces: a predictive theoretical model, J. Chem. Phys. 105 (4) (1996) 1609–1620.
[36] J. Häger, D. Glatzer, H. Kuze, M. Fink, H. Walther, Rotationally excited NO molecules incident on a graphite surface: molecular rotation and translation after scattering, Surf. Sci. 374 (1997) 181–190.
[37] G. Nyman, L. Holmlid, J.B.C. Pettersson, Surface scattering of NO from graphite: a statistical description of energy distributions, J. Chem. Phys. 93 (1) (1990) 845–853.
[38] J. Blömer, A.E. Beylich, Molecular dynamics simulation of energy accommodation of internal and translational degrees of freedom at gas–surface interfaces, Surf. Sci. 423 (1999) 127–133.
[39] D.W. Mackowski, Monte Carlo simulation of hydrodynamics drag and thermophoresis of fractal aggregates of spheres in the free-molecular flow regime, J. Aerosol Sci. 37 (2006) 242–259.
[40] A.V. Filippov, M. Zurita, D.E. Rosner, Fractal-like aggregates: relation between morphology and physical properties, J. Colloid Interface Sci. 229 (2000) 261–273.
[41] R.G. Lord, Application of the Cercignani–Lampis scattering kernel to Direct Simulation Monte Carlo calculations, in: A.E. Beylich (Ed.), Rarefied Gas Dynamics: Proceedings 17th International Symposium on Rarefied Gas Dynamics, Aachen, Germany, 1990, pp. 1427–1433.
[42] R.G. Lord, Application of the two-temperature Maxwellian model to describe re-emission of gas molecules from surfaces, J. Phys. D 25 (1991) 327–330.